



Quantifying choriocapillaris flow deficits using global and localized thresholding methods: a correlation study

Zhongdi Chu¹, Qinqin Zhang¹, Hao Zhou¹, Yingying Shi², Fang Zheng², Giovanni Gregori², Philip J. Rosenfeld², Ruikang K. Wang^{1,3}

¹Department of Bioengineering, University of Washington, Seattle, Washington, USA; ²Department of Ophthalmology, Bascom Palmer Eye Institute, University of Miami Miller School of Medicine, Miami, Florida, USA; ³Department of Ophthalmology, University of Washington, Seattle, Washington, USA

Correspondence to: Ruikang K. Wang. Department of Bioengineering, University of Washington, 3720 15th Ave. NE, Seattle, Washington 98195, USA. Email: wangrk@uw.edu.

Background: To investigate the correlation and agreement of two previously published choriocapillaris (CC) quantification methods using a normal database with swept-source optical coherence tomography angiography (SS-OCTA).

Methods: Normal adult subjects from all age groups imaged by SS-OCTA were used in this study. Each subject was imaged with 3 mm × 3 mm and 6 mm × 6 mm scan patterns centered on fovea, upon which en face CC images were generated by segmenting volumetric OCTA data. After signal compensation and removal of projection artifacts and noise, CC images were analyzed to identify flow deficits (FD) using two published methods. The first method utilized standard deviation from a young normal database (SD method) as the global thresholding while the second method utilized fuzzy C-means algorithm (FCM method) with local thresholding. Both methods segmented FDs from CC images and quantified FD density (FDD) and mean FD size (MFDS). In each 3 mm × 3 mm scan, three regions were quantified: a 1 mm circle (C_1), a 1.5 mm rim ($R_{1.5}$) and a 2.5 mm circle ($C_{2.5}$). In each 6 mm × 6 mm scan, five regions were quantified: C_1 , $R_{1.5}$, $C_{2.5}$, a 2.5 mm rim ($R_{2.5}$) and a 5 mm circle (C_5). Spearman correlation and Bland-Altman plot analyses were conducted to compare the two methods.

Results: Data obtained from 164 normal subjects (age: 56±19, 59% females) were used in this study. Strong correlations were observed between the two methods in all comparisons (r : 0.78–0.94, all $P < 0.0001$). Overall MFDS provided higher or comparable correlation coefficients (r) compared to FDD. We have also observed stronger correlations in the central macula compared to parafoveal and perifoveal regions for both FDD and MFDS. In regions of C_1 , $R_{1.5}$ and $C_{2.5}$, 6 mm × 6 mm scans resulted in better agreement (smaller mean bias, similar or tighter limit of agreement) between the two methods for both FDD and MFDS compared to 3 mm × 3 mm scans.

Conclusions: There are strong correlations and satisfactory agreement between SD method and FCM method. SD method requires the reference to a normal database for CC quantification while FCM does not. Both methods could be used for the analysis of CC FDs in clinical settings depending on specific study designs such as the availability of a normal database.

Keywords: Optical coherence tomography angiography (OCTA); swept source OCTA; choriocapillaris (CC); flow deficits

Submitted Nov 08, 2018. Accepted for publication Dec 12, 2018.

doi: 10.21037/qims.2018.12.09

View this article at: <http://dx.doi.org/10.21037/qims.2018.12.09>

Introduction

Choriocapillaris (CC) plays an important role in multiple disease pathologies such as age-related macular degeneration (AMD), diabetic retinopathy (DR), uveitis, and glaucoma (1-7). Traditional dye-based angiography such as indocyanine green angiography has been used to image CC *in vivo* (8), but the limited resolution of dye based-angiography makes it impossible to achieve the level of CC visualization necessary for accurate quantification. Better visualization of CC *in vivo* and reliable quantification of the CC is needed to improve our understanding of the CC involvement in multiple eye diseases and help facilitate early diagnosis, improve our understanding of disease progression, and monitor treatment.

Recently, optical coherence tomography (OCT) and OCT based angiography (OCTA) (9,10) have been introduced into clinical ophthalmology (11-22). OCTA is a non-invasive, safe, fast, and cost-effective technology that extracts the intrinsic signals due to moving particles, such as red blood cells, in functional vessels to achieve an *in vivo* angiogram. Due to its fast imaging speed (seconds), and high spatial resolution (~15–20 μm laterally, ~6 μm axially), a great deal of effort has been devoted to achieving accurate visualization and quantification of CC with OCTA (23-29). In particular, our group has reported two different methods to segment and quantify flow deficits (FDs) in *en face* CC images with swept-source OCTA (SS-OCTA). The first method (29) utilized a threshold based on the standard deviation (SD) calculated from CC images of 20 eyes randomly chosen from a group of 20–30 years old. This SD method has been used to quantify FDs in the CC in a normal database. One of its potential limitations is that it requires a collection of normal database as the reference. Therefore, it would not be able to directly translate between different scanning protocols, nor from one manufacturer's OCTA system to another. To mitigate this limitation, we have developed an alternative method (30) that utilized a fuzzy C-means (FCM) algorithm to segment and quantify CC. This FCM method was initially developed by Dunn in the early seventies (31) to cluster large datasets into different categories, and now it is widely used in bioinformatics and machine learning. The FCM was used in OCTA to assign each pixel into different memberships (CC flows or CC FDs), based on the histogram of the whole image (30). The advantage of the FCM method is that it can be applied across different OCTA systems or different scanning protocols.

In this study, we compared these two CC quantification methods, the SD method and the FCM method, using a normal database of 164 subjects to determine if the two methods produce comparable quantitative CC parameters. In addition to providing guidance on the use of these algorithms, a good agreement between the two methods would further validate the underlying approach to CC FDs quantification.

Methods

In this study, we used an existing SS-OCTA database available from the University of Miami and the University of Washington. The database was obtained from a cross-sectional, study of normal eyes over a wide range of ages that was approved by the Institutional Review Board of Medical Sciences Subcommittee at University of Miami, Miller School of Medicine. The study at the University of Washington was also approved by the Institutional Review Board of Medical Sciences Subcommittee at University of Washington, Seattle. The tenets of the Declaration of Helsinki and the Health Insurance Portability and Accountability Act of 1996 regulations were followed. Informed consents were obtained from all subjects before participation. Subjects with a normal ocular history, no visual complaints, and no identified optic disc, retinal, or choroidal pathology on examination were enrolled in the study between November 2016 to February 2018. 15 to 25 subjects were included in each decade ranging from 20s to 80s.

For all subjects, both eyes were scanned using the PLEX™ Elite 9000 (Carl Zeiss Meditec, Dublin, CA), and both 3 mm \times 3 mm and 6 mm \times 6 mm SS-OCTA images centered on the fovea were acquired. The right eyes were selected for analysis by default unless poor signal strength (<7) or severe motion artifacts were present. Due to the variability of the OCT signal strength among individual subjects, all the images were normalized to the signal strength of nine before OCTA maps were obtained for further CC analysis (32). A semi-automatic segmentation software (33) was then applied to both the OCT and OCTA images to produce a 20 μm thickness CC slab located beneath Bruch's membrane. *En face* CC flow images were compensated using the corresponding *en face* structural images for any possible signal loss due to overlying anatomy (29). Subsequently, retinal projection artifacts were removed (32) before the CC OCTA images were further processed for quantification.

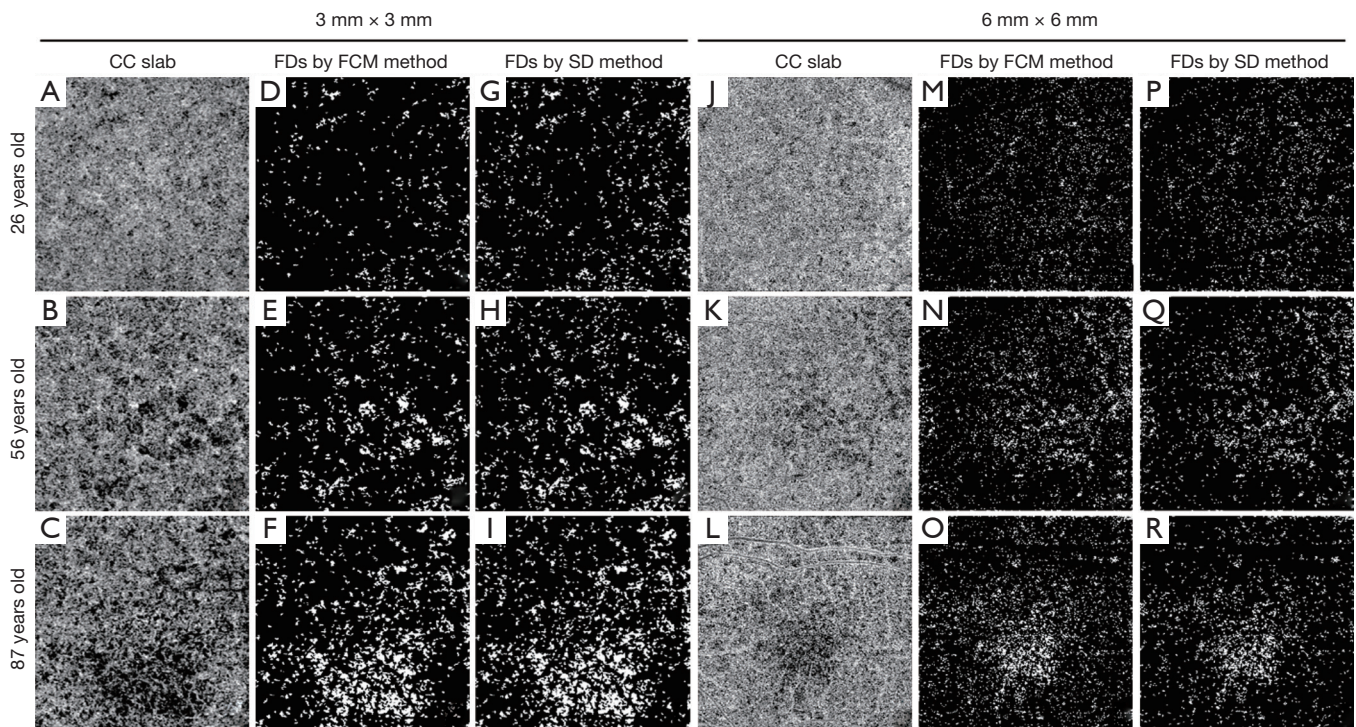


Figure 1 Examples of CC FD segmentations using the SD and FCM methods on 3 mm × 3 mm and 6 mm × 6 mm scans. (A,B,C) 3 mm × 3 mm *en face* CC OCTA images of three subjects of different ages (26, 56, and 87 years old); (D,E,F) corresponding CC FD binary maps produced by the FCM method; (G,H,I) corresponding CC FD binary maps produced by SD method; (J,K,L) 6 mm × 6 mm *en face* CC OCTA images of the same subjects; (M,N,O) corresponding CC FD binary maps produced by FCM method; (P,Q,R) corresponding CC FD binary maps produced by SD method. SD, standard deviation; FCM, fuzzy C-means; OCTA, optical coherence tomography angiography.

Two previously published methods, the SD and FCM methods, were applied to segment FDs (Figure 1). Briefly, in the SD method, the mean and SD from the reference normal database were used to determine a global threshold. Pixels with an intensity lower than one SD below its mean were segmented as FDs. In the FCM method, all pixels were clustered into memberships, CC vasculature and FDs, based on their intensity and the histogram distribution of the whole image. The number of memberships were automatically determined using the elbow method (34) and could vary from image to image. The first membership corresponds to the FDs, as it is the membership with lowest OCTA signal intensities.

Both methods generated CC FD binary maps for all subjects. A final step before the comparison was to remove FDs with an equivalent diameter smaller than 24 μm from the CC FD maps, since these are smaller than the estimated inter-capillary distance (ICD) and are likely to represent noise (30,35). Subsequently, FD density (FDD) and mean FD size (MFDS) (30) were calculated based on the respective

CC FD binary maps (Figure 1D,E,F,G,H,I,M,N,O,P,Q,R). In each 3 mm × 3 mm scan, we quantified three regions centered at the fovea: a 1mm circle (C_1), a 1.5 mm rim ($R_{1.5}$) and a 2.5 mm circle ($C_{2.5}$). Similarly, in each 6 mm × 6 mm scans, we quantified five regions centered at the fovea: C_1 , $R_{1.5}$, $C_{2.5}$, a 2.5 mm rim ($R_{2.5}$) and a 5 mm circle (C_5). Positions of all quantified circles and rims are illustrated in Figure 2. Fovea positions were identified using a method previously described (36).

Statistical analyses were performed using MATLAB (R2016b; MathWorks, Inc., Natick, Massachusetts, USA) and Prism (GRAPHPAD software, San Diego, CA, USA). The nonparametric Spearman correlations and Bland-Altman plots were used to describe the agreement between the methods (37). Repeatability was quantified as the coefficient of variation (CV) (38).

Results

We first used a published dataset of 10 normal subjects

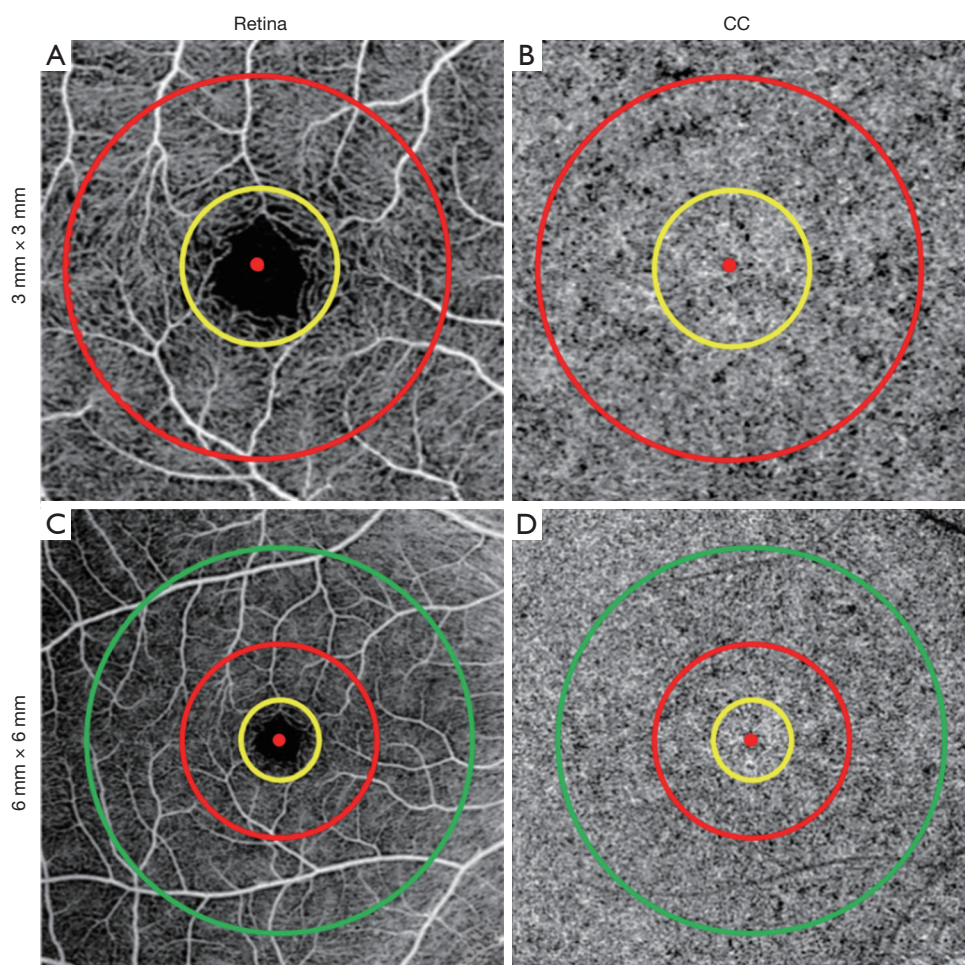


Figure 2 Illustration of the different CC regions that were quantified. (A) 3 mm × 3 mm *en face* retina OCTA image, red dot shows the position of fovea, yellow circle represents the 1 mm diameter circle (C_1) and the red circle represents the 2.5 mm diameter circle ($C_{2.5}$), the 1.5 mm rim ($R_{1.5}$) corresponds to the region between the 1 mm circle (yellow) and the 2.5 mm circle (red). (B) 3 mm × 3 mm *en face* CC OCTA image with the same C_1 , $R_{1.5}$, and $C_{2.5}$ regions. (C) 6 mm × 6 mm *en face* retina OCTA image, red dot shows the position of fovea, green circle represents the 5 mm diameter circle (C_5) and the yellow and red circles correspond to the same C_1 , $R_{1.5}$ and $C_{2.5}$ regions as in A, and the 2.5 mm rim ($R_{2.5}$) corresponds to the region between the 2.5 mm circle (red) and the 5.0 mm circle (green). (D) 6 mm × 6 mm *en face* CC OCTA image with the same C_1 , $R_{1.5}$, $C_{2.5}$, $R_{2.5}$, C_5 regions. OCTA, optical coherence tomography angiography.

and 11 subjects with drusen secondary to AMD (29) to evaluate the intra-visit repeatability of both the SD and FCM methods (Table 1). Repeatability of the SD method and FCM methods was comparable for FDD measurements while the FCM method provided better repeatability for MFDS measurements. Both methods provided better repeatability in the normal subjects group compared with repeatability in the drusen subjects group.

We then used both the SD and FCM methods on a total of 164 eyes from 164 subjects (age: 56 ± 19 , 59% females)

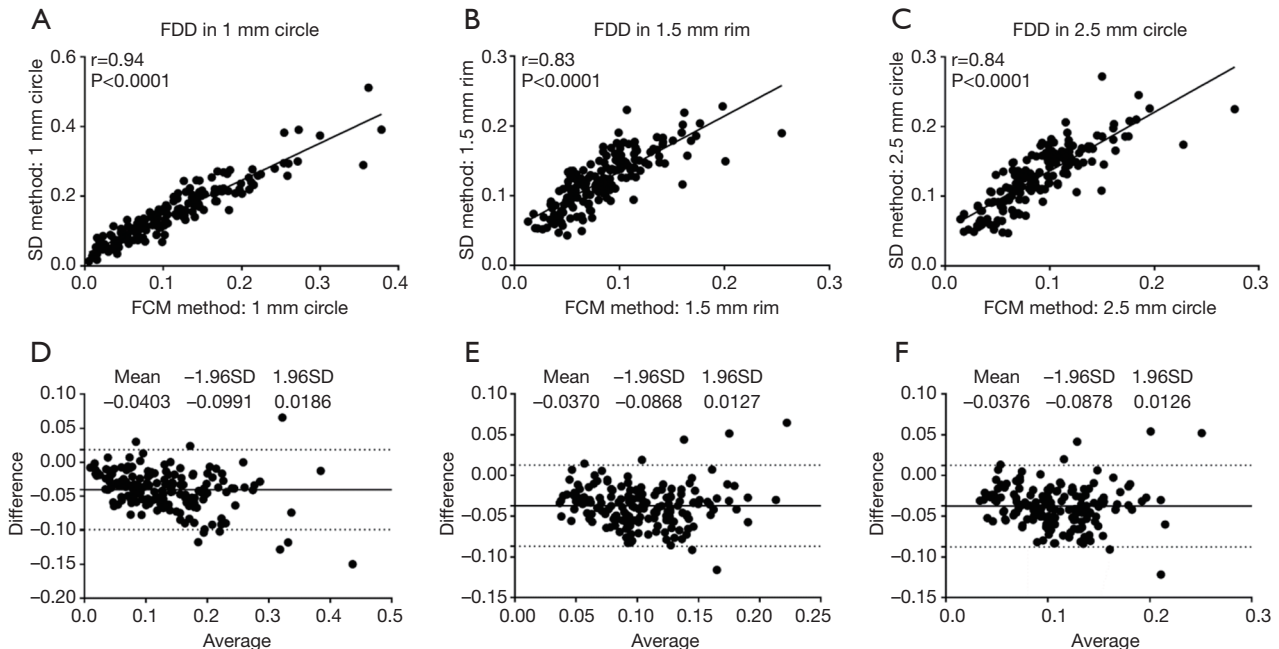
from the normal database. Both 3 mm × 3 mm and 6 mm × 6 mm OCTA datasets were analyzed using both methods for all 164 normal eyes. For the 3 mm × 3 mm scans, FDD and MFDS were measured over three regions (C_1 , $R_{1.5}$, $C_{2.5}$), while for the 6 mm × 6 mm scans, five regions (C_1 , $R_{1.5}$, $R_{2.5}$, $C_{2.5}$, C_5) were used.

To compare quantitative CC measurements of FDD and MFDS produced by two methods, we applied Spearman's correlation analysis and Bland-Altman agreement analysis. Figure 3 demonstrates these analyses of the FDD in the

Table 1 Comparison of intra-visit repeatability of SD method and FCM method

Coefficient of variation	FDD (%)		MFDS (%)	
	SD method	FCM method	SD method	FCM method
Normal	5.68	4.58	4.87	2.80
Drusen	7.43	4.64	7.39	5.04

SD, standard deviation; FCM, fuzzy C-means.

**Figure 3** FDD correlation and agreement analysis of 3 mm × 3 mm scans in C_1 (A,D), $R_{1.5}$ (B,E) and $C_{2.5}$ (C,F).

3 mm × 3 mm scans. The correlation between two methods was the strongest in C_1 ($r=0.94$, $P<0.0001$), followed by $C_{2.5}$ ($r=0.84$, $P<0.0001$) and then $R_{1.5}$ ($r=0.83$, $P<0.0001$). Overall, the FCM method produced lower FDD compared with the SD method. We have observed a mean bias of -0.0403 between the SD method and the FCM method in C_1 , with a limit of agreement (LOA) of -0.0991 to 0.0186 . C_2 has a mean bias of -0.0376 and a LOA of -0.0878 to 0.0126 . In $R_{1.5}$, the mean bias is -0.0370 while the LOA is -0.0868 to 0.0127 . Similar trend was also found in MFDS in the 3 mm × 3 mm scans (Figure 4). The correlation between the two methods was the strongest in C_1 ($r=0.93$, $P<0.0001$), followed by $C_{2.5}$ ($r=0.86$, $P<0.0001$) and then $R_{1.5}$ ($r=0.83$, $P<0.0001$). Overall, the FCM method produced larger MFDS compared with the SD method. There was a mean bias of $327.9 \mu\text{m}^2$ (9.7 pixels) between the SD method

and the FCM method in C_1 [LOA: $-752.2 \mu\text{m}^2$ (21.9 pixels) to $1,478 \mu\text{m}^2$ (43.1 pixels)], a mean bias of $409 \mu\text{m}^2$ (11.9 pixels) in $C_{2.5}$ [LOA: $-303.5 \mu\text{m}^2$ (8.8 pixels) to $1,121 \mu\text{m}^2$ (32.6 pixels)] and a mean bias of $284.6 \mu\text{m}^2$ (8.3 pixels) in $R_{1.5}$ [LOA: $341.9 \mu\text{m}^2$ (9.9 pixels) to $911.1 \mu\text{m}^2$ (26.5 pixels)]. Our data indicate that in the 3 mm × 3 mm scans, the SD method resulted in smaller FDs compared to the FCM method, since the FCM method gave lower FDD yet larger MFDS on average. This suggests that the SD method could be more sensitive to smaller FDs while FCM method is more specific to larger FDs in 3 mm × 3 mm scans.

In the 6 mm × 6 mm scans, similar trends were observed for the correlations between the SD method and FCM method (Figures 5,6). Correlation was stronger in the central macular regions and weaker in parafoveal and perifoveal regions. For FDD in circles (Figure 5), the

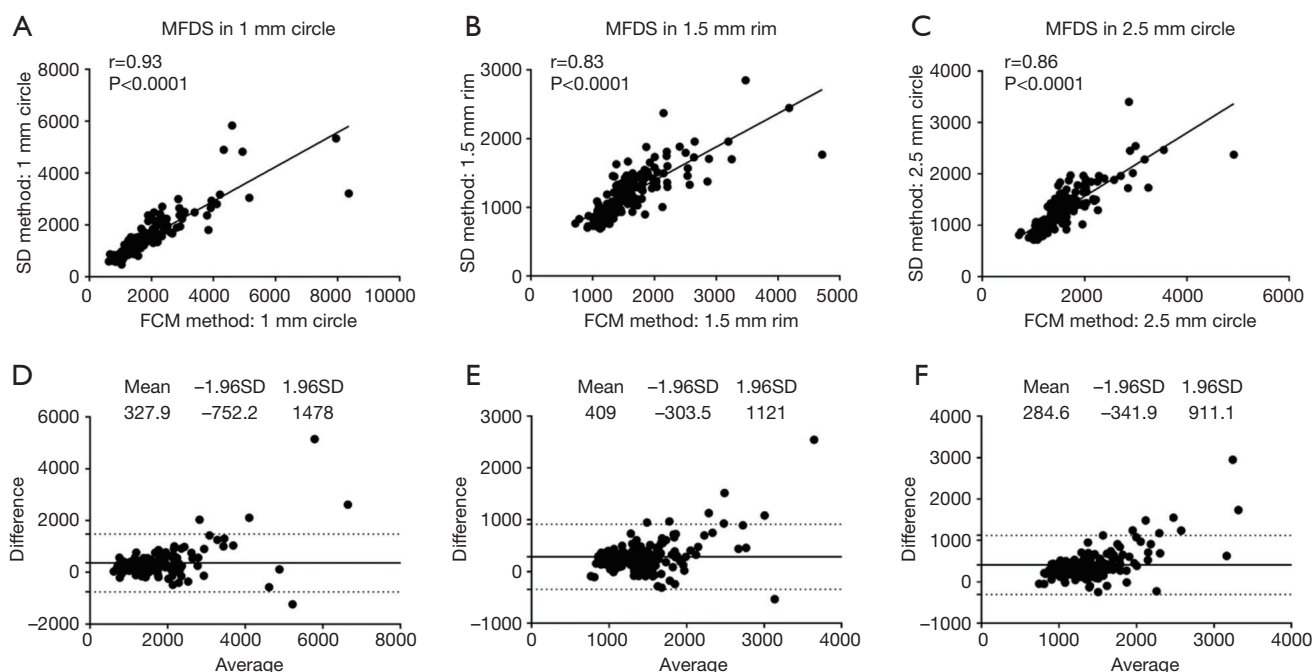


Figure 4 MFDS correlation and agreement analysis of 3 mm × 3 mm scans in C₁ (A,D), R_{1,5} (B,E) and C_{2,5} (C,F).

correlation between two methods was the strongest in the central C₁ (r=0.94, P<0.0001), followed by C_{2,5} (r=0.86, P<0.0001) and then C₅ (r=0.78, P<0.0001). Similarly, in the rims, the R_{1,5} (r=0.85, P<0.0001) showed a stronger correlation than R_{2,5} (r=0.81, P<0.0001). On average, in all five regions, the FCM method resulted in higher FDD compared with the SD method. The mean bias in the C₁ is 0.0188 (LOA: -0.0376 to 0.0752), 0.0212 for C_{2,5} (LOA: -0.0331 to 0.0757) and 0.0198 for C₅ (LOA: -0.0226 to 0.0623). In the rims, the mean bias in R_{1,5} is 0.0218 (LOA: -0.0333 to 0.0769) and 0.0193 for R_{2,5} (LOA: -0.0196 to 0.0583). Similar trends for the correlations were found in MFDS as well (Figure 6). In circles, the correlation was the strongest in C₁ (r=0.93, P<0.0001), followed by C_{2,5} (r=0.90, P<0.0001) then C₅ (r=0.86, P<0.0001). In rims, the correlation was stronger in R_{1,5} (r=0.88, P<0.0001) than R_{2,5} (r=0.85, P<0.0001). Overall, MFDS resulted in stronger correlations in all regions but C₁ when compared with FDD. In terms of differences, the mean bias in C₁ is 73.6 μm² (0.5 pixels) with a LOA of -1,118 μm² (8.1 pixels) to 1,265 μm² (9.2 pixels), for C_{2,5}, the mean bias is 36.5 μm² (0.3 pixels) and the LOA is -669 μm² (4.9 pixels) to 597 μm² (4.3 pixels), for C₅, the mean bias is -116.1 μm² (0.8 pixels) and the LOA is -669 μm² (4.9 pixels) to 597 μm² (4.3 pixels). In rims, the mean bias in R_{1,5} is -116.1 μm² (0.8 pixels) and

the LOA is -669 μm² (4.9 pixels) to 597 μm² (4.3 pixels), for R_{2,5}, the mean bias is -220.2 μm² (1.6 pixels) and the LOA is -615.5 μm² (4.5 pixels) to 175.1 μm² (1.3 pixels).

Discussion

In this study, we have compared two methods for the quantification of CC FDs and found that both the SD and FCM methods provided good repeatability in normal subjects and drusen subjects, with the FCM method resulting in comparable or lower CV. We also demonstrated strong correlations between both methods for the quantitative CC parameters (r: 0.78–0.94, all P<0.0001) derived from various regions of both the 3 mm × 3 mm scans and 6 mm × 6 mm scans. Overall, the MFDS measurements resulted in comparable or better correlations compared to FDD measurements, especially in the 6 mm × 6 mm scans.

Visualizing and quantifying CC have been a keen interest of many investigators (24,25,29,37,39–45), especially since the recent technological advances of commercial OCTA systems. However, researchers should be cautious and vigilant while conducting quantitative analyses of CC using OCTA. There are a number of factors that could potentially compromise the integrity of CC quantification

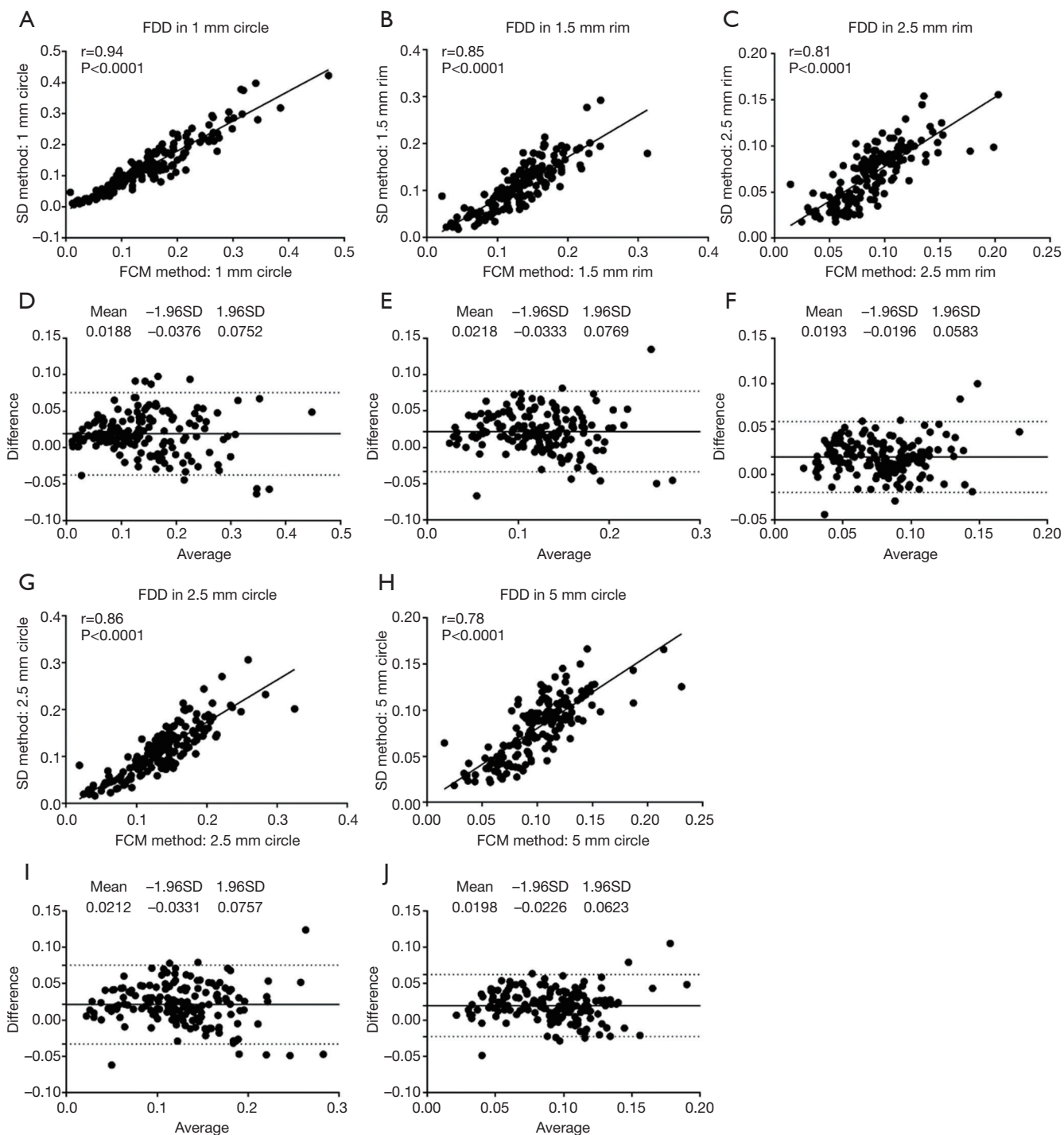


Figure 5 FDD correlation and agreement analysis of 6 mm × 6 mm scans in C_1 (A,D), $R_{1.5}$ (B,E), $R_{2.5}$ (C,F), $C_{2.5}$ (G,I) and C_5 (H,J).

data such as scan signal intensity and strength, CC slab segmentation, CC vasculature (or FDs) segmentation algorithm, and appropriate quantitative parameters (such as FDD and MFDS in this study). In our study, all included

scans had a signal strength index higher than 7 and manual segmentation was employed to ensure correct CC slab. We have also employed a compensation strategy that uses structural OCT signal to correct for attenuated OCTA

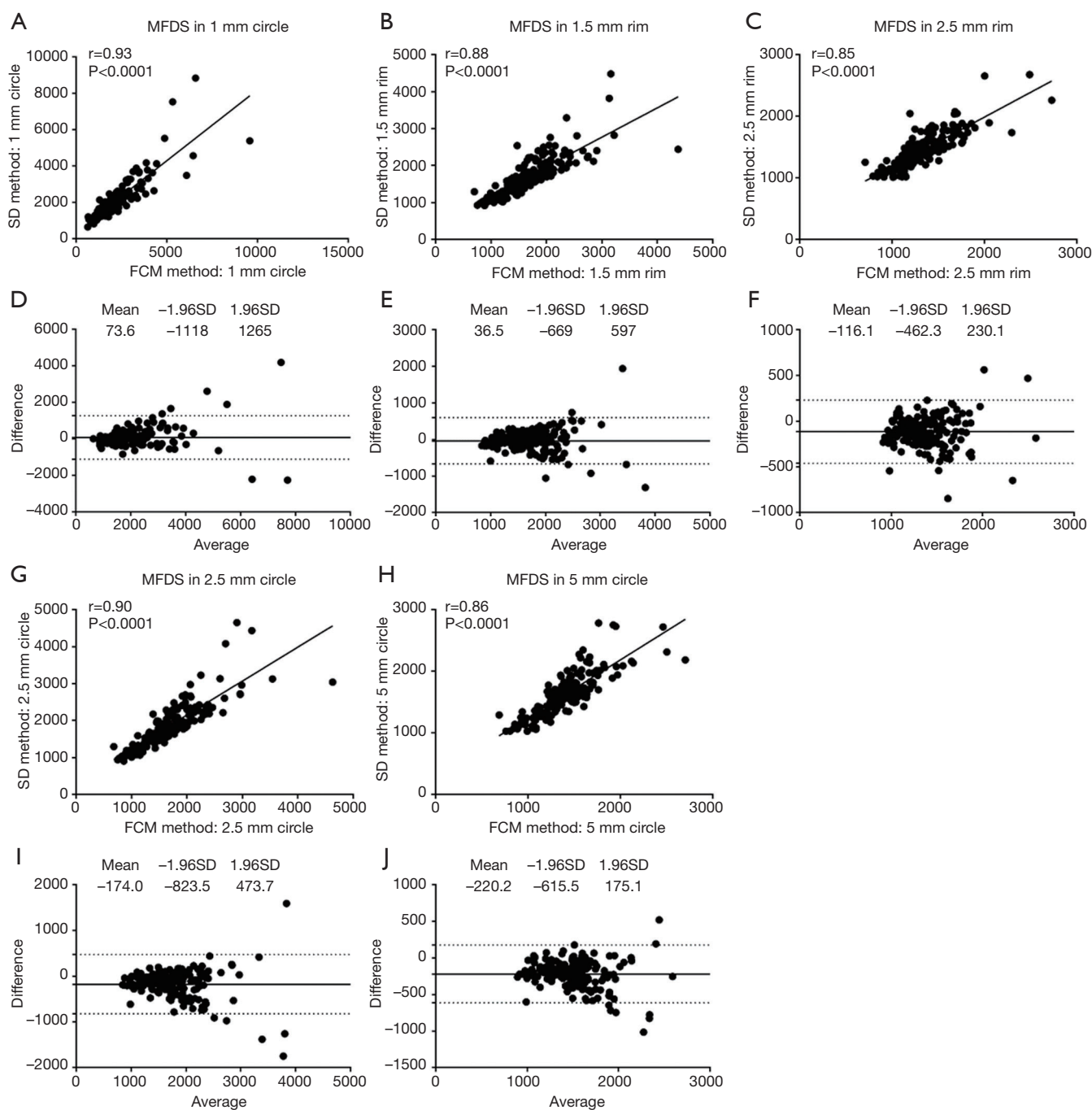


Figure 6 MFDS correlation and agreement analysis of 6 mm × 6 mm scans in C₁ (A,D), R_{1.5} (B,E), R_{2.5} (C,F), C_{2.5} (G,I) and C₅ (H,J).

signals in the CC. Both methods compared in this report showed satisfactory repeatability (FCM method all CV ≤5.04%, SD method all CV ≤7.43%), strong correlations (all P<0.0001, all r>0.83 for 3 mm × 3 mm and all r>0.78 for 6 mm × 6 mm), and good agreement.

In summary, we have demonstrated strong correlations of quantitative CC metrics between the SD and FCM methods. Overall, the correlation was stronger in the central macular regions than in the parafoveal and perifoveal regions. For the same regions (C₁, R_{1.5}, C_{2.5}), 6 mm × 6 mm

scans resulted in similar or stronger correlations compared to 3 mm × 3 mm scans. For either 3 mm × 3 mm or 6 mm × 6 mm scan pattern, the MFDS measurements resulted in comparable or stronger correlations compared with the FDD measurements. In terms of agreement, 6 mm × 6 mm scans resulted in smaller mean biases compared with the same regions (C_1 , $R_{1.5}$, $C_{2.5}$) in the 3 mm × 3 mm scans.

There are several limitations in the current study. Firstly, we lack a ground truth of accepted *in vivo* CC vasculature and FDs measurements for comparison with our quantitative analyses. However, currently there are no clinically available imaging techniques that can provide such a ground truth. It remains possible that future technological developments of adaptive optics OCTA or faster SS-OCTA instruments could solve this problem. Secondly, we only have compared the two methods on a normal population, and we did not include diseased population in the comparison part of this study. Future studies are needed to investigate the correlation and agreement between the SD method and the FCM method in diseased eyes. Regardless of these limitations, strong correlations and satisfactory agreements of quantitative CC parameters using the SD and FCM methods were observed. Both methods could be used for future analyses depending on specific study designs, such as availability of a normal database.

Acknowledgements

Funding: Research supported by grants from the National Eye Institute (R01EY024158, R01EY028753), the Salah Foundation, an unrestricted grant from the Research to Prevent Blindness, Inc., New York, NY, and the National Eye Institute Center Core Grant (P30EY014801) to the Department of Ophthalmology, University of Miami Miller School of Medicine. The funding organization had no role in the design or conduct of this research.

Footnote

Conflicts of Interest: Dr. Gregori, Dr. Wang and Dr. Rosenfeld received research support from Carl Zeiss Meditec, Inc. Dr. Gregori and the University of Miami co-own a patent that is licensed to Carl Zeiss Meditec, Inc. Dr. Rosenfeld is a consultant for Achillion Pharmaceuticals, Acucela, Boehringer-Ingelheim, Carl Zeiss Meditec, Chengdu Kanghong Biotech, Ocunexus Therapeutics, Healios K.K., Hemera Biosciences, F. Hoffmann-La

Roche Ltd., Isarna Pharmaceuticals, Lin Bioscience, NGM Biopharmaceuticals, and Unity Biotechnology. Dr. Rosenfeld has equity interest in Apellis, Digisight, and Ocudyne. Dr. Wang discloses intellectual property owned by the Oregon Health and Science University and the University of Washington. Dr. Wang also receives research support from Tasso Inc., Moptim Inc., and Colgate Palmolive Company. He is a consultant to Insight Photonic Solutions, Kowa, and Carl Zeiss Meditec. The remaining authors have no conflicts of interest to declare.

Ethical Statement: The study was approved by the Institutional Review Board of Medical Sciences Subcommittee at University of Miami, Miller School of Medicine. The study at the University of Washington was also approved by the Institutional Review Board of Medical Sciences Subcommittee at University of Washington, Seattle. The tenets of the Declaration of Helsinki and the Health Insurance Portability and Accountability Act of 1996 regulations were followed. Informed consents were obtained from all subjects before participation.

References

1. Herborg C. Posterior uveitis: new insights provided by indocyanine green angiography. Nature Publishing Group, 1998.
2. Cao J, McLeod DS, Merges CA, Luttj G. Choriocapillaris degeneration and related pathologic changes in human diabetic eyes. Arch Ophthalmol 1998;116:589-97.
3. Luttj G, Grunwald J, Majji AB, Uyama M, Yoneya S. Changes in choriocapillaris and retinal pigment epithelium in age-related macular degeneration. Mol Vis 1999;5:35.
4. Nazari H, Hariri A, Hu Z, Ouyang Y, Sadda S, Rao NA. Choroidal atrophy and loss of choriocapillaris in convalescent stage of Vogt-Koyanagi-Harada disease: in vivo documentation. J Ophthalmic Inflamm Infect 2014;4:9.
5. Whitmore SS, Sohn EH, Chirco KR, Drack AV, Stone EM, Tucker BA, Mullins RF. Complement activation and choriocapillaris loss in early AMD: implications for pathophysiology and therapy. Prog Retin Eye Res 2015;45:1-29.
6. Spraul CW, Lang GE, Lang GK, Grossniklaus HE. Morphometric changes of the choriocapillaris and the choroidal vasculature in eyes with advanced glaucomatous

- changes. *Vision Res* 2002;42:923-32.
7. Chen CL, Bojikian KD, Gupta D, Wen JC, Zhang Q, Xin C, Kono R, Mudumbai RC, Johnstone MA, Chen PP, Wang RK. Optic nerve head perfusion in normal eyes and eyes with glaucoma using optical coherence tomography-based microangiography. *Quant Imaging Med Surg* 2016;6:125.
 8. Piccolino FC, Borgia L. Central serous chorioretinopathy and indocyanine green angiography. *Retina* 1994;14:231-42.
 9. Chen C-L, Wang RK. Optical coherence tomography based angiography. *Biomed Opt Express* 2017;8:1056-82.
 10. Kashani AH, Chen C-L, Gahm JK, Zheng F, Richter GM, Rosenfeld PJ, Shi Y, Wang RK. Optical coherence tomography angiography: A comprehensive review of current methods and clinical applications. *Prog Retin Eye Res* 2017;60:66-100.
 11. Mariampillai A, Leung MK, Jarvi M, Standish BA, Lee K, Wilson BC, Vitkin A, Yang VX. Optimized speckle variance OCT imaging of microvasculature. *Opt Lett* 2010;35:1257-9.
 12. Braaf B, Vienola KV, Sheehy CK, Yang Q, Vermeer KA, Tiruveedhula P, Arathorn DW, Roorda A, de Boer JF. Real-time eye motion correction in phase-resolved OCT angiography with tracking SLO. *Biomed Opt Express* 2013;4:51-65.
 13. Huang Y, Zhang Q, Thorell MR, An L, Durbin MK, Laron M, Sharma U, Gregori G, Rosenfeld PJ, Wang RK. Swept-source OCT angiography of the retinal vasculature using intensity differentiation-based optical microangiography algorithms. *Ophthalmic Surg Lasers Imaging Retina* 2014;45:382-9.
 14. Waheed NK, Moulton EM, Fujimoto JG, Rosenfeld PJ. Optical coherence tomography angiography of dry age-related macular degeneration. *OCT Angiography in Retinal and Macular Diseases*. Karger Publishers, 2016:91-100.
 15. Kim AY, Chu Z, Shahidzadeh A, Wang RK, Puliafito CA, Kashani AH. Quantifying Microvascular Density and Morphology in Diabetic Retinopathy Using Spectral-Domain Optical Coherence Tomography Angiography Quantifying Vascular Changes in DR With SD-OCTA. *Invest Ophthalmol Vis Sci* 2016;57:OCT362-70.
 16. Pakzad-Vaezi K, Khaksari K, Chu Z, Van Gelder RN, Wang RK, Pepple KL. Swept-Source OCT Angiography of Serpiginous Choroiditis. *Ophthalmol Retina* 2018;2:712-9.
 17. Kim AY, Rodger DC, Shahidzadeh A, Chu Z, Koulis N, Burkemper B, Jiang X, Pepple KL, Wang RK, Puliafito CA. Quantifying Retinal Microvascular Changes in Uveitis Using Spectral-Domain Optical Coherence Tomography Angiography. *Am J Ophthalmol* 2016;171:101-12.
 18. Pepple KL, Chu Z, Weinstein J, Munk MR, Van Gelder RN, Wang RK. Use of En Face Swept-Source Optical Coherence Tomography Angiography in Identifying Choroidal Flow Voids in 3 Patients With Birdshot Chorioretinopathy. *JAMA Ophthalmol* 2018;136:1288-92.
 19. Richter GM, Madi I, Chu Z, Burkemper B, Chang R, Zaman A, Sylvester B, Reznik A, Kashani A, Wang RK. Structural and Functional Associations of Macular Microcirculation in the Ganglion Cell-Inner Plexiform Layer in Glaucoma Using Optical Coherence Tomography Angiography. *J Glaucoma* 2018;27:281-90.
 20. Zhang Q, Rezaei KA, Saraf SS, Chu Z, Wang F, Wang RK. Ultra-wide optical coherence tomography angiography in diabetic retinopathy. *Quant Imaging Med Surg* 2018;8:743.
 21. Kam J, Zhang Q, Lin J, Liu J, Wang RK, Rezaei K. Optical coherence tomography based microangiography findings in hydroxychloroquine toxicity. *Quant Imaging Med Surg* 2016;6:178.
 22. Zhang Q, Wang J, Wang RK. Highly efficient eigen decomposition based statistical optical microangiography. *Quant Imaging Med Surg* 2016;6:557.
 23. Spaide RF. Choriocapillaris flow features follow a power law distribution: implications for characterization and mechanisms of disease progression. *Am J Ophthalmol* 2016;170:58-67.
 24. Kurokawa K, Liu Z, Miller DT. Adaptive optics optical coherence tomography angiography for morphometric analysis of choriocapillaris. *Biomed Opt Express* 2017;8:1803-22.
 25. Chu Z, Chen C-L, Zhang Q, Pepple K, Durbin M, Gregori G, Wang RK. Complex signal-based optical coherence tomography angiography enables in vivo visualization of choriocapillaris in human choroid. *J Biomed Opt* 2017;22:1-10.
 26. Choi W, Mohler KJ, Potsaid B, Lu CD, Liu JJ, Jayaraman V, Cable AE, Duker JS, Huber R, Fujimoto JG. Choriocapillaris and choroidal microvasculature imaging with ultrahigh speed OCT angiography. *PloS one* 2013;8:e81499.
 27. Gorczynska I, Migacz J, Jonnal R, Zawadzki R, Poddar R, Werner J. editors. Imaging of the human choroid with a 1.7 MHz A-scan rate FDML swept source OCT system. *Ophthalmic Technologies XXVII*; 2017: International Society for Optics and Photonics.
 28. Uji A, Balasubramanian S, Lei J, Baghdasaryan E,

- Al-Sheikh M, Sadda SR. Choriocapillaris imaging using multiple en face optical coherence tomography angiography image averaging. *JAMA Ophthalmol* 2017;135:1197-204.
29. Zhang Q, Zheng F, Motulsky EH, Gregori G, Chu Z, Chen CL, Li C, de Sisternes L, Durbin M, Rosenfeld PJ, Wang RK. A Novel Strategy for Quantifying Choriocapillaris Flow Voids Using Swept-Source OCT Angiography. *Invest Ophthalmol Vis Sci* 2018;59:203-11.
 30. Chu Z, Zhou H, Cheng Y, Zhang Q, Wang RK. Improving visualization and quantitative assessment of choriocapillaris with swept source OCTA through registration and averaging applicable to clinical systems. *Sci Rep* 2018;8:16826.
 31. Dunn JC. A fuzzy relative of the ISODATA process and its use in detecting compact well-separated clusters. *Journal of Cybernetics* 1973;32-57.
 32. Zhang Q, Zhang A, Lee CS, Lee AY, Rezaei KA, Roisman L, Miller A, Zheng F, Gregori G, Durbin MK, An L, Stetson PF, Rosenfeld PJ, Wang RK. Projection artifact removal improves visualization and quantitation of macular neovascularization imaged by optical coherence tomography angiography. *Ophthalmol Retina* 2017;1:124-36.
 33. Yin X, Chao JR, Wang RK. User-guided segmentation for volumetric retinal optical coherence tomography images. *J Biomed Opt* 2014;19:086020.
 34. Kodinariya TM, Makwana PR. Review on determining number of Cluster in K-Means Clustering. *International Journal* 2013;1:90-5.
 35. Zhang Q, Shi Y, Zhou H, Gregori G, Chu Z, Zheng F, Motulsky EH, De Sisternes L, Durbin M, Rosenfeld PJ, Wang RK. Accurate estimation of choriocapillaris flow deficits beyond normal intercapillary spacing with swept source OCT angiography. *Quant Imaging Med Surg* 2018;8:658.
 36. Wang F, Gregori G, Rosenfeld PJ, Lujan BJ, Durbin MK, Bagherinia H. Automated detection of the foveal center improves SD-OCT measurements of central retinal thickness. *Ophthalmic Surg Lasers Imaging* 2012;43:S32-7.
 37. Altman DG, Bland JM. Measurement in medicine: the analysis of method comparison studies. *The Statistician* 1983;32:307-17.
 38. Bland JM, Altman DG. Measurement error proportional to the mean. *BMJ* 1996;313:106.
 39. Borrelli E, Souied EH, Freund KB, Querques G, Miere A, Gal-Or O, Sacconi R, Sadda SR, Sarraf D. Reduced choriocapillaris flow in eyes with type 3 neovascularization and age-related macular degeneration. *Retina* 2018;38:1968-76.
 40. Moreira-Neto CA, Moulton EM, Fujimoto JG, Waheed NK, Ferrara D. Choriocapillaris Loss in Advanced Age-Related Macular Degeneration. *J Ophthalmol* 2018;2018:8125267.
 41. Al-Sheikh M, Falavarjani KG, Pfau M, Uji A, Le PP, Sadda SR. Quantitative Features of the Choriocapillaris in Healthy Individuals Using Swept-Source Optical Coherence Tomography Angiography. *Ophthalmic Surg Lasers Imaging Retina* 2017;48:623-31.
 42. Klufas MA, Phasukkijwatana N, Iafe NA, Prasad PS, Agarwal A, Gupta V, Ansari W, Pichi F, Srivastava S, Freund KB. Optical coherence tomography angiography reveals choriocapillaris flow reduction in placoid chorioretinitis. *Ophthalmol Retina* 2017;1:77-91.
 43. Gao SS, Patel RC, Jain N, Zhang M, Weleber RG, Huang D, Pennesi ME, Jia Y. Choriocapillaris evaluation in choroideremia using optical coherence tomography angiography. *Biomed Opt Express* 2016;8:48-56.
 44. Spaide RF. Ising model of choriocapillaris flow. *Retina* 2018;38:79-83.
 45. Borrelli E, Shi Y, Uji A, Balasubramanian S, Nassisi M, Sarraf D, Sadda SR. Topographic Analysis of the Choriocapillaris in Intermediate Age-related Macular Degeneration. *Am J Ophthalmol* 2018;196:34-43.

Cite this article as: Chu Z, Zhang Q, Zhou H, Shi Y, Zheng F, Gregori G, Rosenfeld PJ, Wang RK. Quantifying choriocapillaris flow deficits using global and localized thresholding methods: a correlation study. *Quant Imaging Med Surg* 2018;8(10):1102-1112. doi: 10.21037/qims.2018.12.09